

Application of the independent component analysis to the iKAGRA data

T. Akutsu^{1,2}, M. Ando^{3,4,1}, K. Arai⁵, Y. Arai⁵, S. Araki⁶, A. Araya⁷, N. Aritomi³, H. Asada⁸, Y. Aso^{9,10}, S. Atsuta¹¹, K. Awai¹², S. Bae¹³, Y. Bae¹⁴, L. Baiotti¹⁵, R. Bajpai¹⁶, M. A. Barton¹, K. Cannon⁴, E. Capocasa¹, M. Chan¹⁷, C. Chen^{18,19}, K. Chen²⁰, Y. Chen¹⁹, H. Chu²⁰, Y.-K. Chu²¹, K. Craig⁵, W. Creus²¹, K. Doi²², K. Eda⁴, S. Eguchi¹⁷, Y. Enomoto³, R. Flaminio^{23,1}, Y. Fujii²⁴, M.-K. Fujimoto¹, M. Fukunaga⁵, M. Fukushima¹, T. Furuhata²², G. Ge²⁵, A. Hagiwara^{5,26}, S. Haino²¹, K. Hasegawa⁵, K. Hashino²², H. Hayakawa¹², K. Hayama¹⁷, Y. Himemoto²⁷, Y. Hiranuma²⁸, N. Hirata¹, S. Hirobayashi²⁹, E. Hirose⁵, Z. Hong³⁰, B. H. Hsieh³¹, G.-Z. Huang³⁰, P. Huang²⁵, Y. Huang²¹, B. Ikenoue¹, S. Imam³⁰, K. Inayoshi³², Y. Inoue²⁰, K. Ioka³³, Y. Itoh³⁴, K. Izumi³⁵, K. Jung³⁶, P. Jung¹², T. Kaji³⁴, T. Kajita³⁷, M. Kakizaki²², M. Kamiizumi¹², S. Kanbara²², N. Kanda³⁴, S. Kanemura³⁸, M. Kaneyama³⁴, G. Kang¹³, J. Kasuya¹¹, Y. Kataoka¹¹, K. Kawaguchi⁵, N. Kawai¹¹, S. Kawamura¹², T. Kawasaki³, C. Kim³⁹, J. C. Kim⁴⁰, W. S. Kim¹⁴, Y.-M. Kim³⁶, N. Kimura²⁶, T. Kinugawa⁴¹, S. Kirii¹², N. Kita³, Y. Kitaoka³⁴, H. Kitazawa²², Y. Kojima⁴², K. Kokeyama¹², K. Komori³, A. K. H. Kong¹⁹, K. Kotake¹⁷, C. Kozakai⁹, R. Koza⁴³, R. Kumar⁴⁴, J. Kume^{4,3,*}, C. Kuo²⁰, H.-S. Kuo³⁰, S. Kuroyanagi⁴⁵, K. Kusayanagi¹¹, K. Kwak³⁶, H. K. Lee⁴⁶, H. M. Lee^{47,48}, H. W. Lee⁴⁰, R. Lee¹⁹, M. Leonardi¹, C. Lin³⁶, C.-Y. Lin⁴⁹, F.-L. Lin³⁰, G. C. Liu¹⁸, Y. Liu⁵⁰, L. Luo²¹, E. Majorana⁵¹, S. Mano⁵², M. Marchio¹, T. Matsui⁵³, F. Matsushima²², Y. Michimura³, N. Mio⁵⁴, O. Miyakawa¹², A. Miyamoto³⁴, T. Miyamoto⁴³, Y. Miyazaki³, K. Miyo¹², S. Miyoki¹², W. Morii⁵⁵, S. Morisaki⁴, Y. Moriwaki²², T. Morozumi⁵, M. Musha⁵⁶, K. Nagano⁵, S. Nagano⁵⁷, K. Nakamura¹, T. Nakamura⁵⁸, H. Nakano⁵⁹, M. Nakano^{22,5}, K. Nakao⁶⁰, R. Nakashima¹¹, T. Narikawa⁵⁸, L. Naticchioni⁵¹, R. Negishi²⁸, L. Nguyen Quynh⁶¹, W.-T. Ni^{25,62,63},

A. Nishizawa⁴, Y. Obuchi¹, T. Ochi⁵, W. Ogaki⁵, J. J. Oh¹⁴, S. H. Oh¹⁴,
M. Ohashi¹², N. Ohishi⁹, M. Ohkawa⁶⁴, K. Okutomi¹², K. Oohara²⁸,
C. P. Ooi³, S. Oshino¹², K. Pan¹⁹, H. Pang²⁰, J. Park⁶⁵, F. E. Peña
Arellano¹², I. Pinto⁶⁶, N. Sago⁶⁷, M. Saijo⁶⁸, S. Saito¹, Y. Saito¹²,
K. Sakai⁶⁹, Y. Sakai²⁸, Y. Sakai³, Y. Sakuno¹⁷, M. Sasaki⁷⁰, Y. Sasaki⁷¹,
S. Sato⁷², T. Sato⁶⁴, T. Sawada³⁴, T. Sekiguchi⁴, Y. Sekiguchi⁷³, N. Seto⁵⁸,
S. Shibagaki¹⁷, M. Shibata^{33,74}, R. Shimizu¹, T. Shimoda³, K. Shimode¹²,
H. Shinkai⁷⁵, T. Shishido¹⁰, A. Shoda¹, K. Somiya¹¹, E. J. Son¹⁴,
H. Sotani¹, A. Suemasa⁵⁶, R. Sugimoto²², T. Suzuki⁶⁴, T. Suzuki⁵,
H. Tagoshi⁵, H. Takahashi⁷¹, R. Takahashi¹, A. Takamori⁷, S. Takano³,
H. Takeda³, M. Takeda²⁸, H. Tanaka³¹, K. Tanaka³⁴, K. Tanaka³¹,
T. Tanaka⁵, T. Tanaka⁵⁸, S. Tanioka^{1,10}, E. N. Tapia San Martin¹,
D. Tatsumi¹, S. Telada⁷⁶, T. Tomaru¹, Y. Tomigami³⁴, T. Tomura¹²,
F. Travasso^{77,78}, L. Trozzo¹², T. Tsang⁷⁹, K. Tsubono³, S. Tsuchida³⁴,
T. Tsuzuki¹, D. Tuyenbayev²¹, N. Uchikata⁸⁰, T. Uchiyama¹², A. Ueda²⁶,
T. Uehara^{81,82}, S. Ueki⁷¹, K. Ueno⁴, G. Ueshima⁷¹, F. Uraguchi¹,
T. Ushiba⁵, M. H. P. M. van Putten⁸³, H. Vocca⁷⁸, S. Wada³,
T. Wakamatsu²⁸, J. Wang²⁵, C. Wu¹⁹, H. Wu¹⁹, S. Wu¹⁹, W-R. Xu³⁰,
T. Yamada³¹, A. Yamamoto⁶, K. Yamamoto²², K. Yamamoto³¹,
S. Yamamoto⁷⁵, T. Yamamoto¹², K. Yokogawa²², J. Yokoyama^{4,3},
T. Yokozawa¹², T. H. Yoon⁸⁴, T. Yoshioka²², H. Yuzurihara⁵, S. Zeidler¹,
Y. Zhao¹, Z.-H. Zhu⁸⁵ (KAGRA Collaboration)

¹*Gravitational Wave Project Office, National Astronomical Observatory of Japan (NAOJ),
Mitaka City, Tokyo 181-8588, Japan*

²*Advanced Technology Center, National Astronomical Observatory of Japan (NAOJ), , Japan*

³*Department of Physics, The University of Tokyo, Bunkyo-ku, Tokyo 113-0033, Japan*

⁴*Research Center for the Early Universe (RESCEU), The University of Tokyo, Bunkyo-ku,
Tokyo 113-0033, Japan*

⁵*Institute for Cosmic Ray Research (ICRR), KAGRA Observatory, The University of Tokyo,
Kashiwa City, Chiba 277-8582, Japan*

⁶*Accelerator Laboratory, High Energy Accelerator Research Organization (KEK), Tsukuba City,
Ibaraki 305-0801, Japan*

⁷*Earthquake Research Institute, The University of Tokyo, Bunkyo-ku, Tokyo 113-0032, Japan*

⁸*Department of Mathematics and Physics, Hirosaki University, Hirosaki City, Aomori
036-8561, Japan*

⁹*Kamioka Branch, National Astronomical Observatory of Japan (NAOJ), Kamioka-cho, Hida
City, Gifu 506-1205, Japan*

- ¹⁰*The Graduate University for Advanced Studies (SOKENDAI), Mitaka City, Tokyo 181-8588, Japan*
- ¹¹*Graduate School of Science and Technology, Tokyo Institute of Technology, Meguro-ku, Tokyo 152-8551, Japan*
- ¹²*Institute for Cosmic Ray Research (ICRR), KAGRA Observatory, The University of Tokyo, Kamioka-cho, Hida City, Gifu 506-1205, Japan*
- ¹³*Korea Institute of Science and Technology Information (KISTI), Yuseong-gu, Daejeon 34141, Korea*
- ¹⁴*National Institute for Mathematical Sciences, Daejeon 34047, Korea*
- ¹⁵*Department of Earth and Space Science, Graduate School of Science, Osaka University, Toyonaka City, Osaka 560-0043, Japan*
- ¹⁶*School of High Energy Accelerator Science, The Graduate University for Advanced Studies (SOKENDAI), Tsukuba City, Ibaraki 305-0801, Japan*
- ¹⁷*Department of Applied Physics, Fukuoka University, Jonan, Fukuoka City, Fukuoka 814-0180, Japan*
- ¹⁸*Department of Physics, Tamkang University, Danshui Dist., New Taipei City 25137, Taiwan*
- ¹⁹*Department of Physics and Institute of Astronomy, National Tsing Hua University, Hsinchu 30013, Taiwan*
- ²⁰*Department of Physics, Center for High Energy and High Field Physics, National Central University, Zhongli District, Taoyuan City 32001, Taiwan*
- ²¹*Institute of Physics, Academia Sinica, Nankang, Taipei 11529, Taiwan*
- ²²*Department of Physics, University of Toyama, Toyama City, Toyama 930-8555, Japan*
- ²³*Univ. Grenoble Alpes, Laboratoire d'Annecy de Physique des Particules (LAPP), Université Savoie Mont Blanc, CNRS/IN2P3, F-74941 Annecy, France*
- ²⁴*Department of Astronomy, The University of Tokyo, Mitaka City, Tokyo 181-8588, Japan*
- ²⁵*State Key Laboratory of Magnetic Resonance and Atomic and Molecular Physics, Wuhan Institute of Physics and Mathematics (WIPM), Chinese Academy of Sciences, Xiaohongshan, Wuhan 430071, China*
- ²⁶*Applied Research Laboratory, High Energy Accelerator Research Organization (KEK), Tsukuba City, Ibaraki 305-0801, Japan*
- ²⁷*College of Industrial Technology, Nihon University, Narashino City, Chiba 275-8575, Japan*
- ²⁸*Graduate School of Science and Technology, Niigata University, Nishi-ku, Niigata City, Niigata 950-2181, Japan*
- ²⁹*Faculty of Engineering, University of Toyama, Toyama City, Toyama 930-8555, Japan*
- ³⁰*Department of Physics, National Taiwan Normal University, sec. 4, Taipei 116, Taiwan*
- ³¹*Institute for Cosmic Ray Research (ICRR), Research Center for Cosmic Neutrinos (RCCN), The University of Tokyo, Kashiwa City, Chiba 277-8582, Japan*
- ³²*Kavli Institute for Astronomy and Astrophysics, Peking University, , China*
- ³³*Yukawa Institute for Theoretical Physics (YITP), Kyoto University, Sakyou-ku, Kyoto City, Kyoto 606-8502, Japan*
- ³⁴*Graduate School of Science, Nambu Yoichiro Institute of Theoretical and Experimental Physics (NITEP), Osaka City University, Sumiyoshi-ku, Osaka City, Osaka 558-8585, Japan*
- ³⁵*Institute of Space and Astronautical Science (JAXA), Chuo-ku, Sagamihara City, Kanagawa 252-0222, Japan*
- ³⁶*Department of Physics, School of Natural Science, Ulsan National Institute of Science and*

- Technology (UNIST), Ulsan 44919, Korea*
- ³⁷*Institute for Cosmic Ray Research (ICRR), The University of Tokyo, Kashiwa City, Chiba 277-8582, Japan*
- ³⁸*Graduate School of Science, Osaka University, Toyonaka City, Osaka 560-0043, Japan*
- ³⁹*Department of Physics, Ewha Womans University, Seodaemun-gu, Seoul 03760, Korea*
- ⁴⁰*Department of Computer Simulation, Inje University, Gimhae, Gyeongsangnam-do 50834, Korea*
- ⁴¹*Department of Astronomy, The University of Tokyo, Bunkyo-ku, Tokyo 113-0033, Japan*
- ⁴²*Department of Physical Science, Hiroshima University, Higashihiroshima City, Hiroshima 903-0213, Japan*
- ⁴³*Institute for Cosmic Ray Research (ICRR), Research Center for Cosmic Neutrinos (RCCN), The University of Tokyo, Kamioka-cho, Hida City, Gifu 506-1205, Japan*
- ⁴⁴*California Institute of Technology, Pasadena, CA 91125, USA*
- ⁴⁵*Institute for Advanced Research, Nagoya University, Furocho, Chikusa-ku, Nagoya City, Aichi 464-8602, Japan*
- ⁴⁶*Department of Physics, Hanyang University, Seoul 133-791, Korea*
- ⁴⁷*Korea Astronomy and Space Science Institute (KASI), Yuseong-gu, Daejeon 34055, Korea*
- ⁴⁸*Department of Physics and Astronomy, Seoul National University, Gwanak-gu, Seoul 08826, Korea*
- ⁴⁹*National Center for High-performance computing, National Applied Research Laboratories, Hsinchu Science Park, Hsinchu City 30076, Taiwan*
- ⁵⁰*Department of Advanced Materials Science, The University of Tokyo, Kashiwa City, Chiba 277-8582, Japan*
- ⁵¹*Istituto Nazionale di Fisica Nucleare (INFN), Sapienza University, Roma 00185, Italy*
- ⁵²*Department of Mathematical Analysis and Statistical Inference, The Institute of Statistical Mathematics, Tachikawa City, Tokyo 190-8562, Japan*
- ⁵³*School of Physics, Korea Institute for Advanced Study (KIAS), Seoul 02455, Korea*
- ⁵⁴*Institute for Photon Science and Technology, The University of Tokyo, Bunkyo-ku, Tokyo 113-8656, Japan*
- ⁵⁵*Disaster Prevention Research Institute, Kyoto University, Uji City, Kyoto 611-0011, Japan*
- ⁵⁶*Institute for Laser Science, University of Electro-Communications, Chofu City, Tokyo 182-8585, Japan*
- ⁵⁷*The Applied Electromagnetic Research Institute, National Institute of Information and Communications Technology (NICT), Koganei City, Tokyo 184-8795, Japan*
- ⁵⁸*Department of Physics, Kyoto University, Sakyou-ku, Kyoto City, Kyoto 606-8502, Japan*
- ⁵⁹*Faculty of Law, Ryukoku University, Fushimi-ku, Kyoto City, Kyoto 612-8577, Japan*
- ⁶⁰*Graduate School of Science, Nambu Yoichiro Institute of Theoretical and Experimental Physics (NITEP), Osaka City University, Sumiyoshi-ku, Osaka City, Osaka 558-8585, Japan*
- ⁶¹*Department of Physics, University of Notre Dame, Notre Dame, IN 46556, USA*
- ⁶²*Department of Physics, National Tsing Hua University, Hsinchu 30013, Taiwan*
- ⁶³*School of Optical Electrical and Computer Engineering, The University of Shanghai for Science and Technology, , China*
- ⁶⁴*Faculty of Engineering, Niigata University, Nishi-ku, Niigata City, Niigata 950-2181, Japan*
- ⁶⁵*Optical instrument development team, Korea Basic Science Institute, , Korea*
- ⁶⁶*Department of Engineering, University of Sannio, Benevento 82100, Italy*

- ⁶⁷*Faculty of Arts and Science, Kyushu University, Nishi-ku, Fukuoka City, Fukuoka 819-0395, Japan*
- ⁶⁸*Research Institute for Science and Engineering, Waseda University, Shinjuku, Tokyo 169-8555, Japan*
- ⁶⁹*Department of Electronic Control Engineering, National Institute of Technology, Nagaoka College, Nagaoka City, Niigata 940-8532, Japan*
- ⁷⁰*Kavli Institute for the Physics and Mathematics of the Universe (IPMU), Kashiwa City, Chiba 277-8583, Japan*
- ⁷¹*Department of Information & Management Systems Engineering, Nagaoka University of Technology, Nagaoka City, Niigata 940-2188, Japan*
- ⁷²*Graduate School of Science and Engineering, Hosei University, Koganei City, Tokyo 184-8584, Japan*
- ⁷³*Faculty of Science, Toho University, Funabashi City, Chiba 274-8510, Japan*
- ⁷⁴*Max Planck Institute for Gravitational Physics, , Germany*
- ⁷⁵*Faculty of Information Science and Technology, Osaka Institute of Technology, Hirakata City, Osaka 573-0196, Japan*
- ⁷⁶*National Metrology Institute of Japan, National Institute of Advanced Industrial Science and Technology, Tsukuba City, Ibaraki 305-8568, Japan*
- ⁷⁷*University of Camerino, , Italy*
- ⁷⁸*Istituto Nazionale di Fisica Nucleare, University of Perugia, Perugia 06123, Italy*
- ⁷⁹*Faculty of Science, Department of Physics, The Chinese University of Hong Kong, Shatin, N.T., Hong Kong, Hong Kong*
- ⁸⁰*Faculty of Science, Niigata University, Nishi-ku, Niigata City, Niigata 950-2181, Japan*
- ⁸¹*Department of Communications, National Defense Academy of Japan, Yokosuka City, Kanagawa 239-8686, Japan*
- ⁸²*Department of Physics, University of Florida, Gainesville, FL 32611, USA*
- ⁸³*Department of Physics and Astronomy, Sejong University, Gwangjin-gu, Seoul 143-747, Korea*
- ⁸⁴*Department of Physics, Korea University, Seongbuk-gu, Seoul 02841, Korea*
- ⁸⁵*Department of Astronomy, Beijing Normal University, Beijing 100875, China*
- *E-mail: Jun'ya Kume kjun0107@resceu.s.u-tokyo.ac.jp

Abstract

We apply independent component analysis (ICA) to the real data from a gravitational wave detector for the first time. ICA separates various sources of signals from multiple detection channels making use of non-Gaussian nature of the statistical distributions of the sources. Specifically we use the iKAGRA data taken in April 2016, and calculate the correlations between the gravitational wave strain channel and 35 physical environmental channels. Using a couple of seismic channels which are found to be strongly correlated with the strain, we perform ICA. Injecting a sinusoidal continuous signal in the strain channel, we find that ICA recovers correct parameters with enhanced signal-to-noise ratio, which demonstrates usefulness of this method.

1 Introduction

Ever since Einstein found the existence of a gravitational wave solution in his theory of general relativity in 1916, it took exactly a century for mankind to succeed in its direct detection. This delay is primarily due to the fact that the gravitational force is an exceedingly weak force compared with other interactions.

The first detection of a gravitational wave by the advanced Laser Interferometer Gravitational wave Observatory (aLIGO) [1] brought a great impact on science and told the beginning of gravitational wave astronomy. Following aLIGO and advanced Virgo, the large-scale cryogenic gravitational wave telescope (LCGT) now known as KAGRA, has been constructed in Kamioka, Japan [2]. KAGRA will play very important roles in the international network of gravitational wave detection by measuring the number of polarization property, which is indispensable to prove the general relativity, and by improving the sky localization of each event significantly. As the first underground and cryogenic detector, it will also provide important information to the third-generation detectors.

Because gravity is the weakest force among the four elementary interactions, gravitational waves have high penetrating power. Therefore, they enable us to see deep inside dense matter, such as neutron stars, and bring information that electromagnetic waves cannot. On the other hand, this property makes its detection very difficult. It is very important to develop methods for extraction of these tiny signals. If the detector noises are normally distributed, the appropriate analysis methods, such as matched filtering [3], are known. However, the problem is not so simple, as it is known that there exist non-Gaussian noises in real data. They decrease the performance of the analysis methods assuming Gaussianity of the noises. What is worse, these noises may be mistaken for true signals and increase the false alarm probability. It is necessary to deal with non-Gaussianity properly as stressed in [4].

In this situation, independent component analysis (ICA) [5, 6, 7] occupies a unique position among methods of signal extraction because it makes use of non-Gaussianity of signals and noises instead of treating it an obstacle. In this paper we report the results of application of ICA to the iKAGRA data and discuss its usefulness in gravitational wave data analysis. This method assumes only statistical independence of the noises and does not impose any other conditions on their distributions.

The rest of the paper is organized as follows. In §2, we introduce ICA in the simplest case only one environmental channel is incorporated to the strain channel and review analytic formulas obtained in our previous paper [8]. In §3, we present our application of ICA to the iKAGRA data with injected artificial continuous signal. The final section §4 is devoted to conclusion.

2 Independent Component Analysis (ICA)

As is seen in our previous paper [4], signal detection under non-Gaussian noises is much more involved than the case with Gaussian since the optimal statistic has much compli-

cated forms. Independent component analysis is an attractive method of signal extraction because it makes use of non-Gaussian nature of the signals [5, 6, 7] (see [9, 10] for textbooks).

Here we consider the following simple problem as a first step to test applicability of this approach for detection of GWs. Let us consider the case where we have two detector outputs, $x_1(t)$ and $x_2(t)$ (t stands for the time). The former is the output from the laser interferometer, namely, the strain channel, and the latter is an environmental channel such as an output of a seismograph. We wish to separate gravitational wave signal $h(t)$ and non-Gaussian noise $k(t)$ using the data of ${}^t\mathbf{x}(t) = (x_1(t), x_2(t))$.

As the simplest case we assume that there is a linear relation between the outputs and the sources:

$$\mathbf{x}(t) = \begin{pmatrix} x_1(t) \\ x_2(t) \end{pmatrix} = A\mathbf{s}(t), \quad \mathbf{s}(t) = \begin{pmatrix} s_1(t) \\ s_2(t) \end{pmatrix} = \begin{pmatrix} h(t) \\ k(t) \end{pmatrix}, \quad (1)$$

where A is assumed to be a time independent matrix.

By definition the gravitational wave signal obeys a probability distribution function (PDF)

$$r_1(h, t) = \delta(h - h(t, \theta)) \quad (2)$$

where $h(t, \theta)$ is the actual waveform of gravitational radiation emitted from some source, where θ collectively denotes parameters of the source. On the other hand, we do not specify the PDF of $k(t)$, $r_2(s_2)$, except that it is a super-Gaussian distribution such as a Poisson distribution with a larger tail than Gaussian.

The detector output of a laser interferometer, of course, suffers from Gaussian noises $n(t)$ besides non-Gaussian noise $k(t)$. Hence, Eq. (1) should actually read

$$\mathbf{x}(t) = A\mathbf{s}(t) + \mathbf{n}(t), \quad \mathbf{n}(t) = \begin{pmatrix} n(t) \\ 0 \end{pmatrix}. \quad (3)$$

Here we have not incorporated any Gaussian noise to the second line where the signal $k(t)$ itself consists of (non-Gaussian) noises and any Gaussian noise can be incorporated to a part of it.

Following [8], we introduce a trick to replace the original source $s_1(t) = h(t)$ by $s_1(t) = h(t) + n(t)$, that is, we regard the Gaussian noise as a part of the original signal. Since $n(t)$ is a Gaussian with vanishing mean, its statistical property is entirely characterized by the two-point correlation function $K(t - t') = \langle n(t)n(t') \rangle$. Then the marginal distribution function of $s_1(t)$ is given by

$$r_1[s_1(t)] = \frac{1}{\sqrt{2\pi\sigma}} \exp \left[-\frac{1}{2\sigma^2} (s_1(t) - h(t, \theta))^2 \right], \quad \sigma^2 = K(0). \quad (4)$$

Thus $s_1(t)$ now satisfies a simple Gaussian distribution which is much easier to handle with than the delta-function distribution (2), and $\mathbf{s}(t)$ and $\mathbf{x}(t)$ are related by a simple formula $\mathbf{x}(t) = A\mathbf{s}(t)$.

Now our goal is to find the inverse matrix of A whose components are not known precisely. One may set it as

$$A = \begin{pmatrix} a_{11} & a_{12} \\ 0 & a_{22} \end{pmatrix}, \quad (5)$$

since the gravitational wave is so weak that it will not affect any environmental meters such as a seismograph. The aim of ICA is to find a linear transformation

$$\mathbf{y} = W\mathbf{x}, \quad (6)$$

such that two components of the transformed variables \mathbf{y} are statistically independent of each other. Thanks to the assumption (5), the matrix W also takes a form

$$W = \begin{pmatrix} w_{11} & w_{12} \\ 0 & w_{22} \end{pmatrix}. \quad (7)$$

If we knew all the components of A , the matrix W could simply be given by the inverse matrix $W = A^{-1}$, in which case we would find $\mathbf{y} = \mathbf{s}$. However, since we do not know it, we attempt to determine W in such a way that the components of \mathbf{y} , $y_1(t)$ and $y_2(t)$ to be statistically independent as much as possible.

In general, mutual independence of statistical variables may be judged by introducing a cost function $L(W)$ which represents a ‘‘distance’’ in the space of statistical distribution functionals. In [8] the Kullback-Leibler divergence [11], which is defined between two arbitrary PDFs $p(\mathbf{y})$ and $q(\mathbf{y})$ as

$$D[p(\mathbf{y}); q(\mathbf{y})] = \int p(\mathbf{y}) \ln \frac{p(\mathbf{y})}{q(\mathbf{y})} d\mathbf{y} = E_{p_y} \left[\ln \frac{p(\mathbf{y})}{q(\mathbf{y})} \right], \quad (8)$$

was adopted to obtain a matrix which realizes statistical independence between y_1 and y_2 . Here $E_p[\cdot]$ denotes an expectation value with respect to a PDF p . Ideally, the matrix W should be found in such a way that the distance between the distribution of \mathbf{y} , $p_y(\mathbf{y})$, which is constructed from the observed distribution function of \mathbf{x} through the linear transformation $\mathbf{y} = W\mathbf{x}$ as

$$p_y(\mathbf{y}) \equiv ||W^{-1}||p_x(\mathbf{x}), \quad (9)$$

and the real distribution function of statistically independent source variables \mathbf{s} , $r(\mathbf{s}) = r_1[s_1(t)]r_2[s_2(t)]$, is minimal. Here $||X||$ denotes the determinant of a matrix X . However, since we do not know the form of $r(\mathbf{s})$ a priori, we minimize the cost function

$$L_q(W) = D[p_y(\mathbf{y}); q(\mathbf{y})] = -H[\mathbf{x}] - \ln ||W|| - E_{p_y} [\ln q(\mathbf{y})], \quad (10)$$

where $q(\mathbf{y}) = q_1(y_1)q_2(y_2)$ is an appropriately chosen distribution function, to find the matrix W [8]. In fact, it is known that even for an arbitrary choice of $q(\mathbf{y})$, the real W gives an extremum of $L_q(W)$. In the above expression (10), $H[\mathbf{x}]$ denotes the entropy of the distribution of \mathbf{x} defined by $H[\mathbf{x}] \equiv -E_{p_x}[\ln p(\mathbf{x})]$, which can be obtained from

observed distribution and has nothing to do with the matrix W . From $\frac{\partial L_q(W)}{\partial w_{ij}} = 0$, we find

$$\sum_j \frac{\partial L_q(W)}{\partial w_{ij}} w_{jk} = E_{p_y} \left[y_k \frac{\partial \ln q(\mathbf{y})}{\partial y_i} \right] + \delta_{ki} = 0, \quad (11)$$

we can solve for the components of W , w_{ij} .

While the solution of Eq. (11) has been obtained in [8], we can show that the same expression can be obtained for our particular problem with $a_{21} = w_{21} = 0$ more easily as we show below.

2.1 Correlation method

From now on we replace the ensemble average $E[\cdot]$ by temporal average of observed values of \mathbf{x} which we denote by brackets.

From

$$\begin{pmatrix} y_1(t) \\ y_2(t) \end{pmatrix} = \begin{pmatrix} w_{11} & w_{12} \\ 0 & w_{22} \end{pmatrix} \begin{pmatrix} x_1(t) \\ x_2(t) \end{pmatrix} = \begin{pmatrix} w_{11}x_1(t) + w_{12}x_2(t) \\ w_{22}x_2(t) \end{pmatrix}, \quad (12)$$

and

$$\begin{pmatrix} x_1(t) \\ x_2(t) \end{pmatrix} = \begin{pmatrix} a_{11} & a_{12} \\ 0 & a_{22} \end{pmatrix} \begin{pmatrix} s_1(t) \\ s_2(t) \end{pmatrix} = \begin{pmatrix} a_{11}s_1(t) + a_{12}s_2(t) \\ a_{22}s_2(t) \end{pmatrix}, \quad (13)$$

we find $y_2(t) = w_{22}x_2(t) = w_{22}a_{22}s_2(t) = w_{22}a_{22}k(t)$ consists of an environmental channel only, while $y_1(t)$ depends both on strain and seismic channels. In order to guarantee statistical independence we need to satisfy $\langle y_1(t)y_2(t) \rangle = 0$, which is equivalent to requiring

$$\langle y_1(t)x_2(t) \rangle = w_{11}\langle x_1(t)x_2(t) \rangle + w_{12}\langle x_2^2(t) \rangle = 0. \quad (14)$$

We therefore obtain

$$w_{12} = -\frac{\langle x_1x_2 \rangle}{\langle x_2^2 \rangle} w_{11}. \quad (15)$$

Since ICA does not uniquely determine the overall factor of \mathbf{y} by nature, this relation suffices for our purpose to determine y_1 . These are what we calculated in our previous paper [8].

Here we develop three components method for further analysis and we apply this method in §3.2.2. This is achieved by the analogy of the GramSchmidt process which is a method for orthonormalising a set of vectors, and it can be extended to the case where there are more than three components. For three components, $\mathbf{y}(t)$ and $\mathbf{x}(t)$ become

$$\begin{pmatrix} y_1(t) \\ y_2(t) \\ y_3(t) \end{pmatrix} = \begin{pmatrix} w_{11} & w_{12} & w_{13} \\ 0 & w_{22} & w_{23} \\ 0 & w_{32} & w_{33} \end{pmatrix} \begin{pmatrix} x_1(t) \\ x_2(t) \\ x_3(t) \end{pmatrix} = \begin{pmatrix} w_{11}x_1(t) + w_{12}x_2(t) + w_{13}x_3(t) \\ w_{22}x_2(t) + w_{23}x_3(t) \\ w_{32}x_2(t) + w_{33}x_3(t) \end{pmatrix}, \quad (16)$$

and

$$\begin{pmatrix} x_1(t) \\ x_2(t) \\ x_3(t) \end{pmatrix} = \begin{pmatrix} a_{11} & a_{12} & a_{13} \\ 0 & a_{22} & a_{23} \\ 0 & a_{32} & a_{33} \end{pmatrix} \begin{pmatrix} s_1(t) \\ s_2(t) \\ s_3(t) \end{pmatrix} = \begin{pmatrix} a_{11}s_1(t) + a_{12}s_2(t) + a_{13}s_3(t) \\ a_{22}s_2(t) + a_{23}s_3(t) \\ a_{32}s_2(t) + a_{33}s_3(t) \end{pmatrix}. \quad (17)$$

Because of the gauge degree of freedom, we can take $w_{32} = 0$ without loss of generality and choose

$$y_3(t) = \tilde{x}_3(t) \equiv \frac{x_3(t)}{\sqrt{\langle x_3^2 \rangle}}. \quad (18)$$

We first require $\langle y_2(t)y_3(t) \rangle = \langle y_2(t)x_3(t) \rangle = 0$. This gives following relation,

$$w_{23} = -\frac{\langle x_2x_3 \rangle}{\langle x_3^2 \rangle}w_{22}. \quad (19)$$

Based on this, we can choose

$$y_2(t) = \tilde{x}_2(t) \equiv \frac{x_2'(t)}{\sqrt{\langle x_2'^2 \rangle}}, \quad x_2'(t) \equiv x_2(t) - \frac{\langle x_2x_3 \rangle}{\langle x_3^2 \rangle}x_3(t). \quad (20)$$

If we take

$$y_1(t) = x_1(t) - \langle x_1\tilde{x}_2 \rangle\tilde{x}_2(t) - \langle x_1\tilde{x}_3 \rangle\tilde{x}_3(t), \quad (21)$$

$\langle y_1(t)y_2(t) \rangle = \langle y_2(t)y_3(t) \rangle = \langle y_3(t)y_1(t) \rangle = 0$ is satisfied. Note that Eq. (21) is symmetrical with respect to the permutation of $x_2(t)$ and $x_3(t)$.

2.2 FastICA method

Next we introduce another method to obtain a matrix W called FastICA [12] which can be easily implemented even when $\mathbf{x}(t)$ has more than two components. In this method, assuming that each component, $s_i(t)$, of source vector $\mathbf{s}(t)$ is properly normalized with vanishing mean, we first apply whitening to the detector outputs $\mathbf{x}(t)$ and take the dispersion of each source $s_i(t)$ to be unity. This is achieved in the following way. First let the normalized eigenvector and corresponding eigenvalue of a matrix $\langle \mathbf{x}^t \mathbf{x} \rangle$ be \mathbf{c}_i and λ_i , respectively ($i = 1, 2, \dots$), and define a matrix Γ by $\Gamma = (\mathbf{c}_1, \mathbf{c}_2, \mathbf{c}_3, \dots)$, and $\Lambda^{-1/2}$ by $\Lambda^{-1/2} = \text{diag}(\lambda_1^{-1/2}, \lambda_2^{-1/2}, \dots)$. Then the whitened variable $\tilde{\mathbf{x}}(t)$ is defined by

$$\tilde{\mathbf{x}}(t) = \Lambda^{-1/2} {}^t \Gamma \mathbf{x} = \Lambda^{-1/2} {}^t \Gamma A \mathbf{s} \equiv \tilde{A} \mathbf{s}, \quad (22)$$

which satisfies

$$\langle \tilde{\mathbf{x}}(t) {}^t \tilde{\mathbf{x}}(t) \rangle = \langle \tilde{A} \mathbf{s} {}^t (\tilde{A} \mathbf{s}) \rangle = \tilde{A} \langle \mathbf{s} {}^t \mathbf{s} \rangle {}^t \tilde{A} = \tilde{A} {}^t \tilde{A} = E. \quad (23)$$

Here we have used the statistical independence of each component of the normalized source term s_i . This means that the matrix \tilde{A} is an orthogonal matrix and that W may be identified with ${}^t \tilde{A}$ for whitened output data $\tilde{\mathbf{x}}$. Thus we may restrict W to be an orthogonal matrix, too, after appropriate whitening¹.

¹Note that this whitening has nothing to do with the whitening of strain data in frequency domain.

Then choosing $q(\mathbf{y})$ as a product of marginal distributions,

$$q(\mathbf{y}) = \tilde{p}_y(\mathbf{y}) \equiv \prod_i \tilde{p}_i(y_i), \quad \tilde{p}_i(y_i) = \int p_y(\mathbf{y}) dy_1 \dots dy_{i-1} dy_{i+1} \dots, \quad (24)$$

the cost function reads

$$L_{\tilde{p}}(W) = D[p_y(\mathbf{y}); \tilde{p}_y(\mathbf{y})] = -H[\mathbf{x}] - \ln \|W\| + \sum_i H_i[y_i], \quad (25)$$

where $H_i[y_i] \equiv - \int dy_i \tilde{p}_i(y_i) \ln \tilde{p}_i(y_i)$ is the entropy of the marginal distribution of y_i . When W is an orthonormal matrix, only the last term matters to determine W . Hence minimization of the cost function for W is achieved by minimizing entropy of the marginal distribution of each variable. This is the spirit of the FastICA method. It has been proposed to maximize the negentropy defined by

$$J[y_i] \equiv H[\nu] - H[y_i], \quad (26)$$

which is a positive semi-definite quantity, instead of the entropy itself. Here ν is a random Gaussian variable with vanishing mean and unit variance.

In order to achieve easier implementation of the method, however, we minimize a simpler cost function $L(\mathbf{w}_i)$ for each row vector \mathbf{w}_i constituting the matrix W as $W \equiv (\mathbf{w}_1, \mathbf{w}_2, \dots)$. Since W is an orthogonal matrix now, we find $|\mathbf{w}_i|^2 = 1$, so the cost function may be defined as

$$L(\mathbf{w}_i) = \{E[G(y_i)] - E[G(\nu)]\}^2 - \beta [|\mathbf{w}_i|^2 - 1], \quad (27)$$

where G is an appropriate nonquadratic function and β is a Lagrange multiplier. Minimization of Eq. (27) corresponds to solving the following equation:

$$E[\tilde{\mathbf{x}} g({}^t \mathbf{w}_i \tilde{\mathbf{x}})] - \beta \mathbf{w}_i = 0, \quad (28)$$

where $g(y) = G'(y)$. FastICA solves for this equation starting from an arbitrary initial choice of \mathbf{w}_i in terms of the Newton method.

Several other methods of ICA have also been tested using mock data without incorporating environmental channels [13].

3 Analysis of iKAGRA data

The initial engineering run of KAGRA without the cryogenic system was done in March and April, 2016 [14]. From the results of many time series data we analyzed, we report those of two datasets of 224 second long. One starts from 20:15:11 UTC on April 14, 2016. The other starts from 01:01:35 UTC on April 17, 2016. For each dataset, we calculated correlation between the strain channel and each of 35 physical environmental monitor

(PEM) channels. We found that almost all of these channels strongly correlated for the latter dataset (strongly correlated data) and weakly correlated for the former dataset (weakly correlated data)².

The amplitude spectrum density (ASD) of strain for each data set is depicted in Fig. 1.

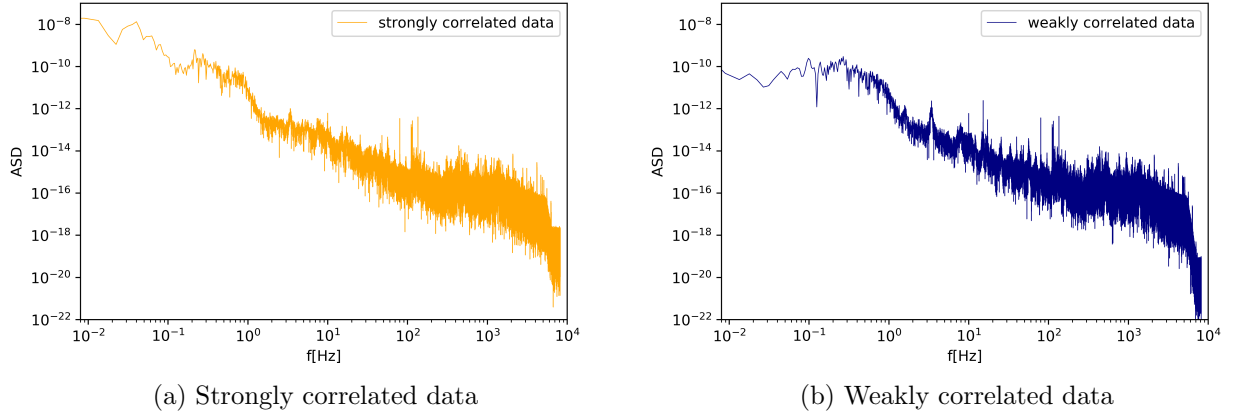


Figure 1: ASD of strain for two datasets. For strongly correlated data, ASD below 0.1Hz becomes much larger than that of weakly correlated data. This means that strongly correlated data is contaminated by seismic noise with low frequency.

We chose two channels which showed large correlation for each dataset. Those channels are listed in Table 1.

Table 1: Correlation between PEM channels and strain.

dataset	channel	correlation coefficient
strongly correlated	PEM-EX_SEIS_Z_SENSINF_OUT16 (4724ch)	-0.6409
	PEM-EY_SEIS_WE_SENSINF_OUT16 (4823ch)	0.5892
weakly correlated	PEM-EX_SEIS_Z_SENSINF_OUT16 (4724ch)	0.3078
	PEM-EY_SEIS_NS_SENSINF_OUT16 (4774ch)	-0.2312

For both dataset, 4724ch had the largest correlation with the strain. This channel is the output of the seismograph that observes vertical vibration installed at the end of the X arm. Both 4774ch and 4823ch are the outputs of seismographs installed at the end of the Y arm, and they observe horizontal vibration orthogonal to each other.

We have made mock strain data injecting sinusoidal continuous waves

$$s(t) = A \sin(2\pi ft), \tag{29}$$

²In this paper we have selected these environment channels based on Pearson’s correlation with the strain. Nonetheless, the correlation does not capture noise sources that contribute to channel data in a nonlinear manner. We defer nonlinear extension of our analysis to future work.

to the strain channel and applied two methods of ICA, which were introduced in the previous section, to this mock data and those environmental channels.

We utilized the python implementation of FastICA from `scikit-learn`.³ We found that results often depend on initial conditions where the Newton method is started. To mitigate this, we parallelly generated thirty realizations and chose one which gives the highest SNR.

3.1 Global performance

First, we analyze how the signal-to-noise ratio (SNR) changes before and after noise separation by ICA for mock data with varying frequencies f . We performed matched filter (MF) analysis to both the raw mock strain data and the noise-removed data in terms of the two methods of ICA using 4724ch as an environmental channel. For various f , we calculated SNR by applying MF with the same frequency as the injected signal. We simultaneously plot the results against the data before and after ICA to assess the global performance of ICA. For strongly correlated data, the results are shown in Fig. 2.

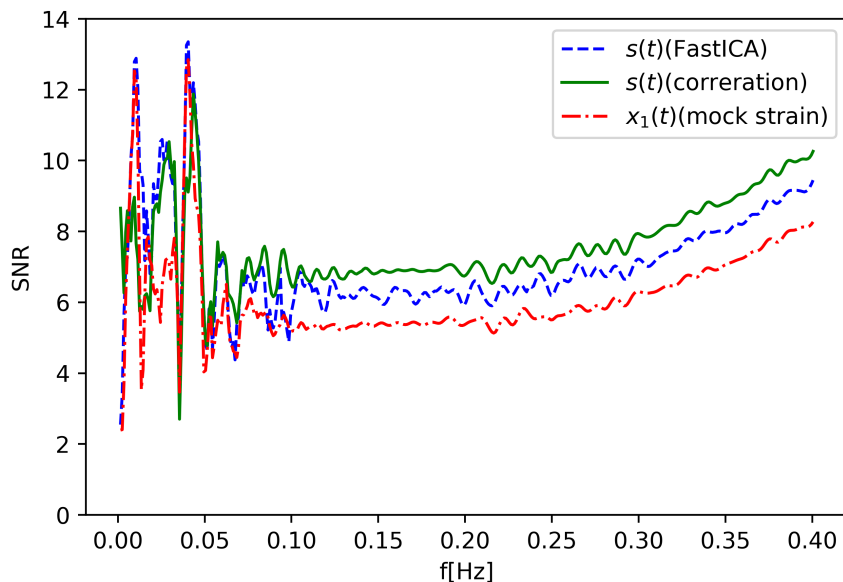


Figure 2: SNR for varying f with and without ICA using 4724ch for the strongly correlated dataset. Red line corresponds to the raw mock strain, while green and blue lines are noise-removed data using the correlation method and FastICA, respectively.

In this dataset, strain had larger amplitude than the other dataset, and we set $A = 9 \times 10^{-10}$. As one can see from Fig. 2, SNRs are homogeneously enhanced by ICA for $f \gtrsim 0.1\text{Hz}$. Correlation method enhances the SNR more than FastICA. However, there are

³<https://scikit-learn.org/stable/>

anomalous peaks at frequencies 0.01Hz and 0.04Hz. As shown in Fig. 1(a), even in the absence of injection strain has large amplitude at these frequencies, which is predominantly contributed by seismic noises. We also found that their oscillation phases are more or less stable during the time period we analyzed. Such noises are difficult to be differentiated from our sinusoidal signal waveform and hence yield large SNR of mock strain as shown in Fig. 2. This however indicates that by removing contribution of the noises, the SNR can possibly be reduced rather than enhanced provided the injected signal is moderate. This is actually realized in the analysis based on the correlation method as seen in Fig. 2.

On the other hand, in the case of FastICA, the reduction of SNR is not seen. This is solely due to our implementation, which tries to increase the SNR as much as possible as mentioned before. In that sense, around the 0.01Hz and 0.04Hz peaks, blue line in Fig. 2 corresponds to the SNR of the separated noise.

Apart from these low frequencies contaminated by seismic noises, we find that ICA improves SNR significantly throughout the entire frequency range with $f \gtrsim 0.1\text{Hz}$. However, based on these considerations, it is deduced that ICA works even near the peak due to seismic noise.

For weakly correlated data, the results are shown in Fig. 3. The amplitude of strain at this time period is moderate, and we set $A = 3 \times 10^{-11}$. As is seen in Fig. 3, the SNR of the data with ICA is higher than the mock data in several frequency ranges. Comparing FastICA with the correlation method, correlation method has fewer frequencies where the SNR falls below that of mock data.

As for weakly correlated data, 4774ch had the second highest correlation with strain. If we use 4774ch instead of 4724ch as the environmental data, the result changes as shown in Fig. 4. Compared with the case 4724ch is used (Fig. 3), the frequency region where the SNR rises is different. As a whole the improvement of SNR is less significant, which is a natural result considering that the correlation coefficient of 4774ch is smaller than that of 4724ch.

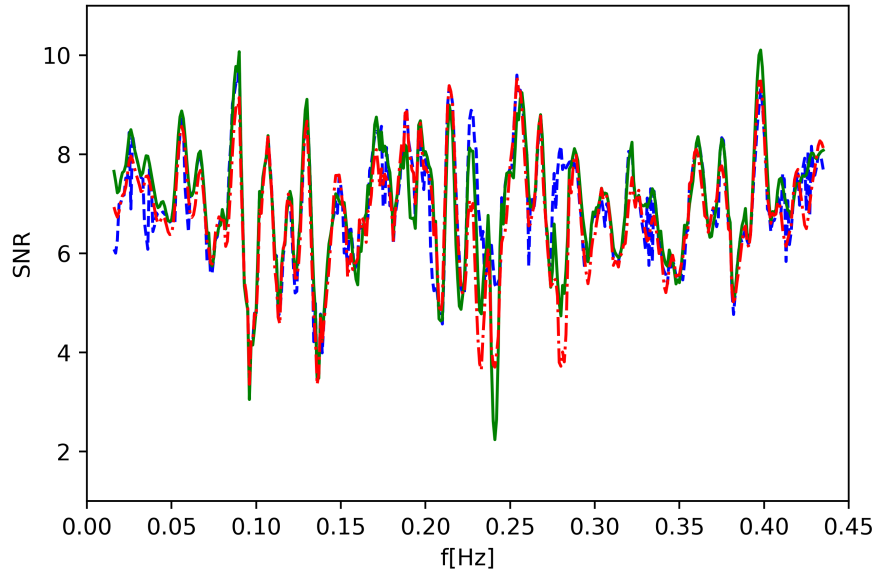


Figure 3: The same figure as in Fig. 2 but for the weakly correlated dataset.

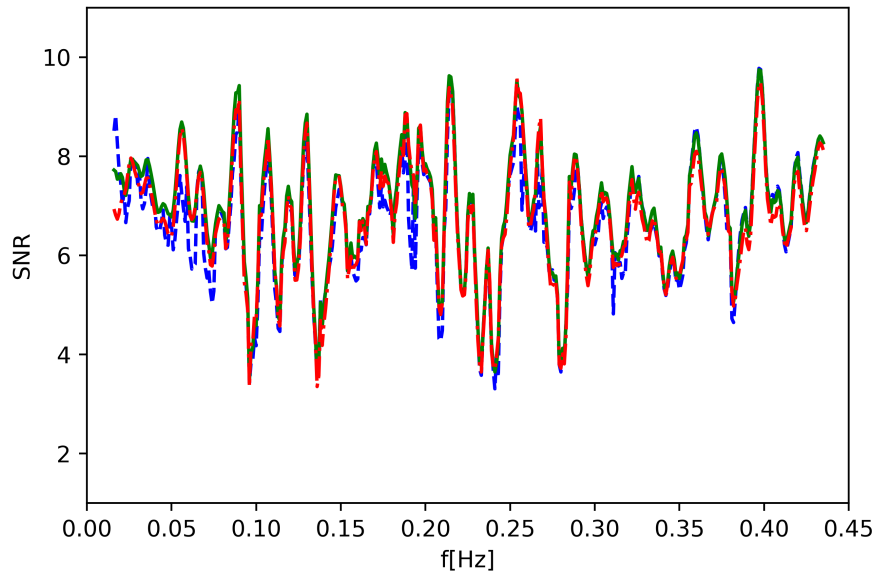


Figure 4: Same as in Fig. 3 but using 4774ch.

3.2 Parameter estimation for strongly correlated data

3.2.1 Two channels ICA

Next, we perform parameter estimation using strongly correlated data to examine whether ICA can recover correct parameters of injected signal. We injected the signal wave form in Eq. (29) with $f = 0.125\text{Hz}$ and $A = 1.3 \times 10^{-9}$. We applied MF analysis to search for the frequency with the highest SNR which corresponds to the maximum likelihood estimation of the parameter. We compare how the result of parameter estimation changes before and after ICA and how much the SNR changes.

Figure 5 depicts the SNR before and after applying ICA.

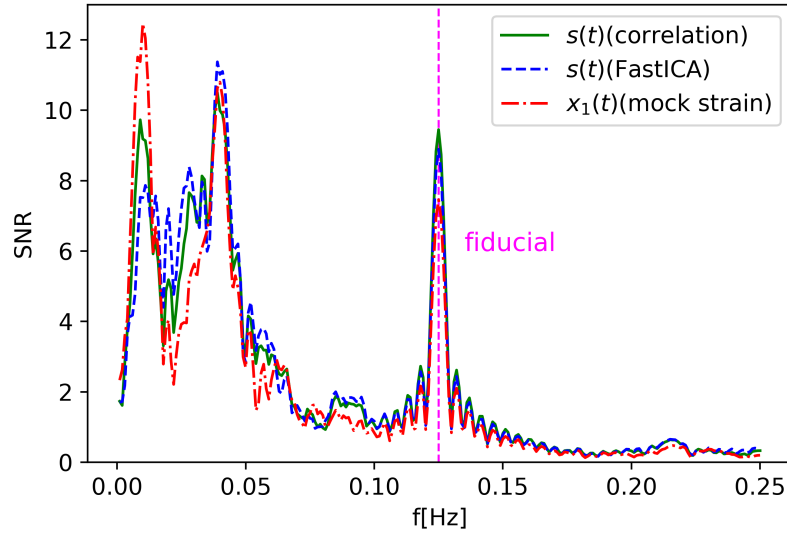


Figure 5: Parameter estimation with fiducial frequency $f=0.125\text{Hz}$. Correspondence of each line is the same as in Fig. 2.

In this case, we can see the effect of seismic noise directly. By ICA with 4724ch, SNR at $f \sim 0.01\text{Hz}$ is reduced and that at the injected frequency $f = 0.125\text{Hz}$ is successfully enhanced. From this result, we deduce that 4724ch is highly correlated to the 0.01Hz peak. On the other hand, the peak of 0.04Hz is still higher, which turned out to be correlated to 4823ch which had second largest correlation with the strain, as we will see below.

3.2.2 Multiple channels ICA

Correlation method

As is seen §3.1, the correlation method shows more stable performance than FastICA, although it is much simpler. This method can be generalized to multi-channel analysis. As a first step to multi-channel analysis, here we investigate the effectiveness of three

components analysis, which we developed in §2.1, including two PEM channels which strongly correlated to the strain. For this purpose we have used the mock data including the same signal wave as in the previous subsection, and applied the three components correlation method to this mock data, 4724ch and 4823ch. The result is depicted in Fig. 6. We simultaneously plotted the results of two components analysis in which we used 4724ch and 4823ch respectively.

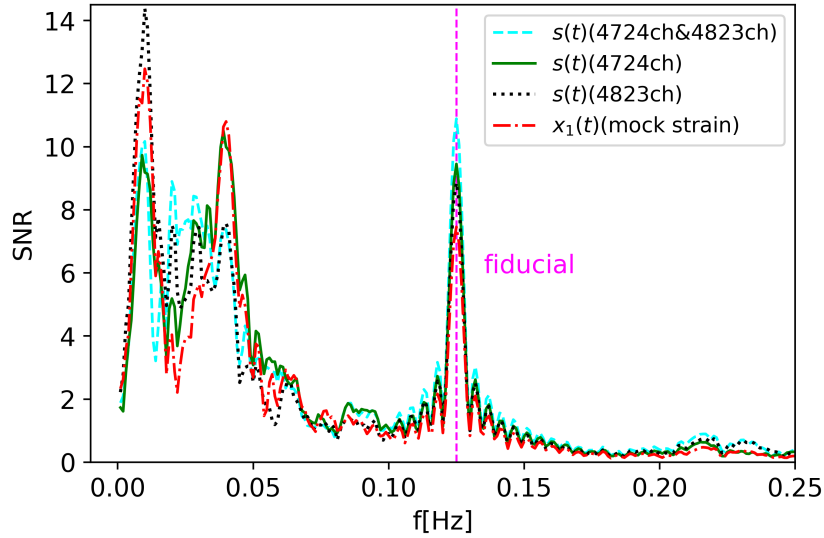


Figure 6: Parameter estimation with multiple channels ICA(correlation method).

The green and black lines correspond to the cases where noises are removed using one PEM channel. While the 0.01Hz peak was reduced by using 4724ch, the 0.04Hz peak was reduced by using 4823ch. However, both peaks can not be reduced by only using one channel. The data with ICA using two PEM channels (cyan line) has much higher SNR than the data with ICA using only one PEM channel. In addition, we successfully reduced both 0.01Hz peak and 0.04Hz peak. This result suggests that by combining many environmental channels we can effectively remove noises with various characteristic frequencies.

FastICA

As explained in §2.2, FastICA can be easily implemented even when there are more than two components. We applied FastICA to the mock data, 4724ch and 4823ch simultaneously. Here, mock data included the same sinusoidal signal as in the previous section. The result is shown in Fig. 7.

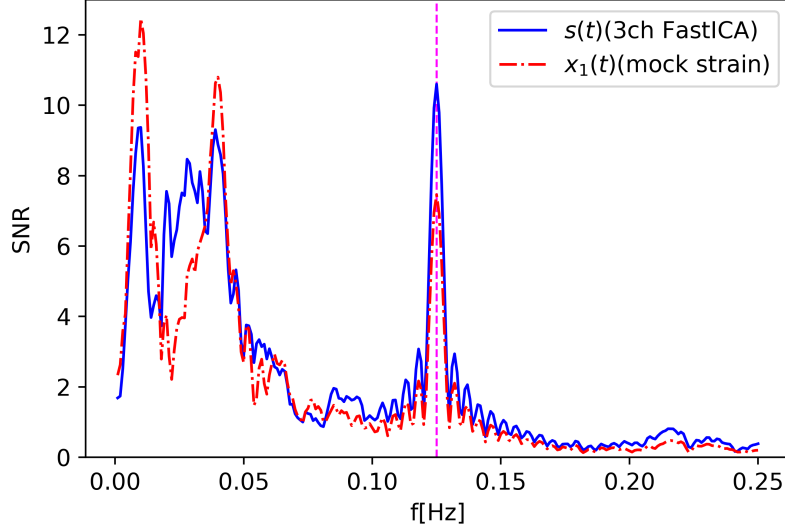


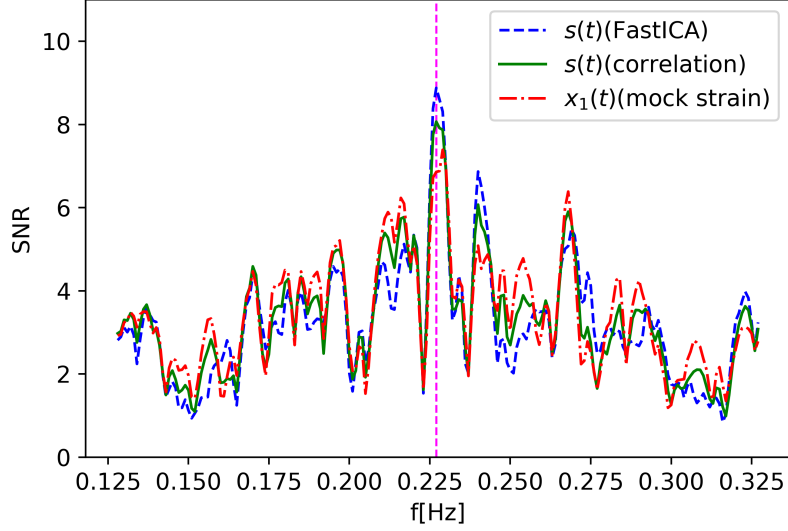
Figure 7: Parameter estimation with multiple channels ICA(FastICA).

As compared to Fig. 5, SNR at fiducial frequency is much higher than the case where only 4724ch was used. This result suggests that the use of multiple environmental channels can enhance the effect of FastICA noise separation. However, compared to the case of the three components correlation method, 3ch FastICA can remove only a small amount of noise at the 0.04Hz peak and SNR at fiducial frequency is lower than that with the correlation method (10.60 for FastICA, 10.89 for correlation method). This indicates that correlation method is more effective than FastICA for this dataset.

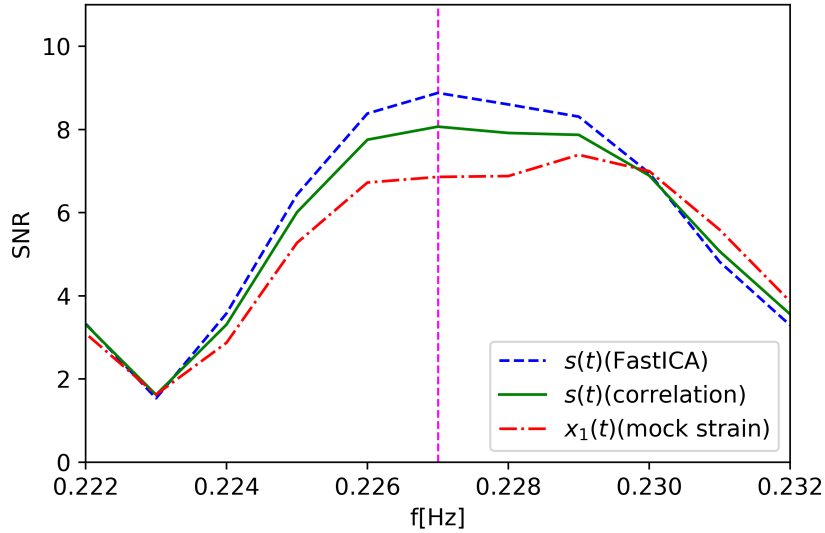
3.3 Parameter estimation for weakly correlated data

We also perform parameter estimation for weakly correlated data. Here, we used 4724ch as an environmental channel. From Fig.3, ICA using 4724ch is most effective for $f = 0.227\text{Hz}$ with this dataset. We injected sinusoidal wave signal with $f = 0.227\text{Hz}$ and $A = 3 \times 10^{-11}$. Again, we applied MF to search for the frequency with the highest SNR. The result is depicted in Fig. 8.

The red line represents SNR calculated with the raw mock strain. The green and blue lines correspond to the noise-removed strain by the correlation method and FastICA, respectively. An enlarged figure of the fiducial ($f = 0.227\text{Hz}$) area is shown in Fig. 8 (b).



(a) Overall view of the result.



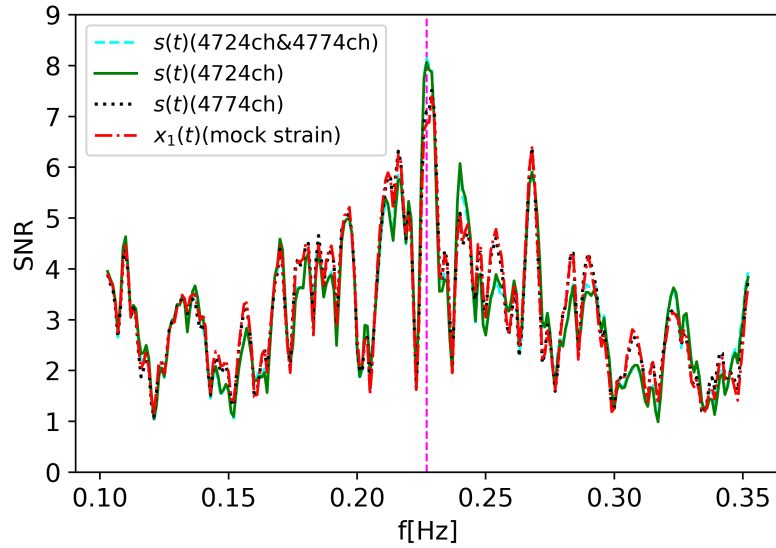
(b) Around the fiducial frequency.

Figure 8: Parameter estimation for weakly correlated data with fiducial frequency $f=0.227\text{Hz}$.

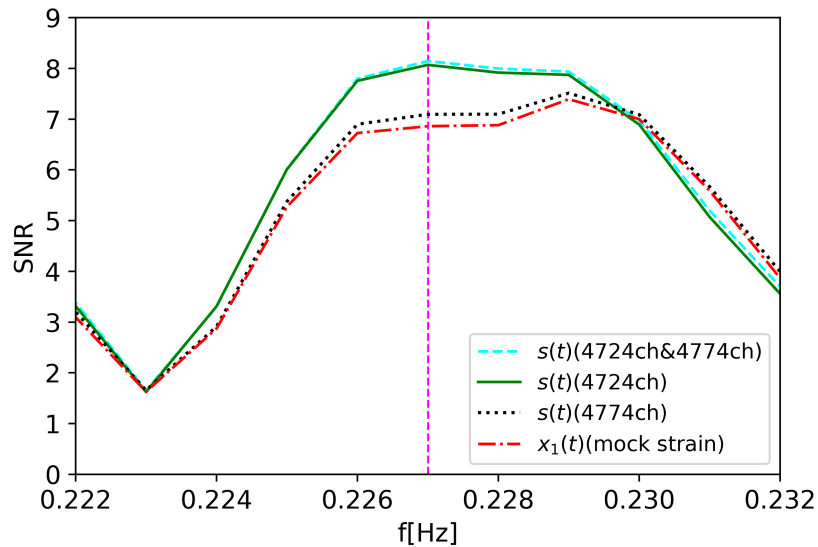
As one can see, in the case of the raw mock strain, the position of the SNR peak deviates from the fiducial one. On the other hand, after applying ICA, the SNR is increased and the peak is found at the correct frequency.

Next, we applied multiple channels ICA for this data using 4724ch and 4774ch. Here, we

used correlation method. Figure 9 depicts the results of analysis. The enlarged figure of the fiducial area is shown in Fig. 9 (b).



(a) Overall view of the result.



(b) Around the fiducial frequency.

Figure 9: Parameter estimation with multiple channels ICA(correlation method)

The green and black lines correspond to the data with ICA using one PEM channel. When using only 4774ch, enhancement of SNR is small and still the SNR peak deviates

from the fiducial frequency. However, the data with ICA using two channels has slightly higher SNR at correct frequency than the data with ICA using only 4724ch. This result for weakly correlated data also supports our expectation that the effect of ICA can be enhanced by combining many environmental channels.

4 Conclusion

In the present paper, we have demonstrated usefulness of ICA in gravitational wave data analysis in application to the iKAGRA strain and environmental channels. Assuming continuous waves as input signal, we have shown that ICA can enhance SNR in particular when the strain channel has large correlation with environmental ones. Moreover, we have shown that ICA can correctly recover input frequencies in parameter estimation. We have also found that combining multiple environmental channels can enhance the effect of ICA. In this paper we analyzed low frequency range mainly because iKAGRA measured mostly the low frequency seismic noises due to the simplified vibration isolation system compared with the full designed specification which will be realized with bKAGRA. Another reason is that only PEM channels measuring low frequency part were available for iKAGRA. These two problems will be solved in bKAGRA with improved vibration isolation system and various PEM channels, and we should be able to apply ICA in the hectoHertz frequency range relevant to GW physics. We will analyze O3 KAGRA data and apply ICA to them.

Acknowledgements

This work was supported by MEXT, JSPS Leading-edge Research Infrastructure Program, JSPS Grant-in-Aid for Specially Promoted Research 26000005, JSPS Grant-in-Aid for Scientific Research on Innovative Areas 2905: JP17H06358, JP17H06361 and JP17H06364, JSPS Core-to-Core Program A. Advanced Research Networks, JSPS Grant-in-Aid for Scientific Research (S) 17H06133, the joint research program of the Institute for Cosmic Ray Research, University of Tokyo, National Research Foundation (NRF) grant of Korea and Computing Infrastructure Project of KISTI-GSDC in Korea, the LIGO project, and the Virgo project. This paper carries JGW Document Number JGW-P1910218.

Jun'ya Kume is supported by a research program of the Leading Graduate Course for Frontiers of Mathematical Sciences and Physics (FMSP). This work was partially supported by JSPS KAKENHI, Grant-in-Aid for Scientific Research No. 15H02082 (Jun'ichi Yokoyama, Yosuke Itoh, Toyokazu Sekiguchi).

References

- [1] B.P. Abbott et al. (LIGO Scientific Collaboration and Virgo Collaboration) Observation of Gravitational Waves from a Binary Black Hole Merger. *Phys. Rev. Lett.*

- 116**, 061102 (2016)
- [2] Y. Aso et al (KAGRA collaboration) Interferometer design of the KAGRA gravitational wave detector. *Phys. Rev. D* **88**, 043007 (2013).
 - [3] L.S. Finn, Detection, measurement, and gravitational radiation. *Phys. Rev. D* **46**, 5236 (1992).
 - [4] J. Yokoyama, Toward the detection of gravitational waves under non-Gaussian noises I. Locally optimal statistic. *Proc. Japan Acad. B* **90**, 422 (2014).
 - [5] Jutten, C. and Herault, J. (1991) Blind separation of sources, Part I: An adaptive algorithm based on neuromimetic architecture. *Signal Processing* **24**, 1.
 - [6] Comon, P. (1994) Independent component analysis, a new concept ? *Signal Processing* **36**, 287.
 - [7] Amari, S. and Cardoso, J.-F. (1997) Blind Source Separation—Semiparametric Statistical Approach. *IEEE Trans. Signal Processing* **45**, 2692.
 - [8] S. Morisaki, J. Yokoyama, K. Eda and Y. Itoh, Toward the detection of gravitational waves under non-Gaussian noises II. Independent Component Analysis. *Proc. Japan Acad. B* **92**, 336 (2016) [arXiv:1605.01983 [gr-qc]].
 - [9] Hyvärinen, A., Karhunen, J., and Oja, E. (2001) *Independent Component Analysis*. John Wiley, New York.
 - [10] Cichocki, A. and Amari, S. (2002) *Adaptive Blind Signal and Image Processing*. John Wiley, New York.
 - [11] Kullback, S. and Leibler, R.A. (1952) On Information and Sufficiency. *Annals of Mathematical Statistics* **22**, 79.
 - [12] A. Hyvärinen, Fast and robust fixed-point algorithms for independent component analysis. *IEEE Trans. Neural Networks* **10**, 626 (1999).
 - [13] R. De Rosa, L. A. Forte, F. Garufi, and L. Milano, Improvement of the performance of a classical matched filter by an independent component analysis preprocessing. *Phys. Rev. D* **85**, 042001 (2012).
 - [14] T. Akutsu *et al.* [KAGRA Collaboration], Construction of KAGRA: an Underground Gravitational Wave Observatory. *PTEP* **2018**, no. 1, 013F01 (2018) [arXiv:1712.00148 [gr-qc]].